

# Opaque phases in type-II chondrules from CR2 chondrites: Implications for CR parent body formation

Devin L. Schrader<sup>a,\*</sup>, Harold C. Connolly Jr.<sup>a,b,c</sup>, Dante S. Lauretta<sup>a</sup>

<sup>a</sup> *University of Arizona, Lunar and Planetary Laboratory, Tucson, AZ 85721, USA*

<sup>b</sup> *Department of Physical Sciences, Kingsborough Community College of the City University of New York, 2001 Oriental Boulevard, Brooklyn, NY 100235, USA*

<sup>c</sup> *Department of Earth and Planetary Sciences, American Museum of Natural History, Central Park West, New York, NY 110024, USA*

Received 18 February 2008; accepted in revised form 17 September 2008; available online 23 September 2008

## Abstract

We report the results of a detailed study of sulfide-bearing opaque assemblages from the MAC 87320, EET 92011, and Renazzo CR carbonaceous chondrites. The objectives of this study are to (1) characterize sulfide and associated phases within CR2 chondrites; (2) determine the petrographic relationship between sulfides, metals, and chondrules; (3) constrain the history of type-II chondrules; (4) ascertain the environments in which type-II chondrules formed and were altered; and (5) unravel the formation and alteration history of the CR parent body as recorded in sulfide-bearing assemblages. Sulfide-bearing opaque assemblages occur primarily within type-II (FeO-rich) chondrules. The sulfide assemblages are concentrated near the chondrule edges. Assemblages in MAC 87320 are composed of troilite, phosphate, and Ni-rich metal. EET 92011 contains assemblages composed of pentlandite, troilite, and Ni-rich metal. The assemblages in Renazzo contain tochilinite, magnetite, troilite, pentlandite, and phosphate. In all of the assemblages in Renazzo the tochilinite is fine grained and intimately mixed with troilite, pentlandite, or magnetite. Opaque assemblages in CR chondrites record a complex history that includes both high- and low-temperature processes. The morphology and composition of sulfides in CR2 chondrites suggests that the sulfide-bearing assemblages originally formed in gas–solid reactions in the nebula at temperatures above the Fe–FeS eutectic (988 °C). Many of the assemblages were subsequently aqueously altered on the CR-chondrite parent body to various degrees at temperatures from ~50 to 200 °C. We combine these observations and interpretations to provide a detailed model of the history of the CR parent body.

© 2008 Elsevier Ltd. All rights reserved.

## 1. INTRODUCTION

The Renazzo meteorite was first identified as distinct from other carbonaceous chondrites by Nelen et al. (1975). It is the type sample for the Renazzo-like carbonaceous chondrite (CR) group, which was first recognized by McSween (1979) and defined by Weisberg et al. (1993). The CR chondrites contain type-I (FeO-poor) and type-II (FeO-rich) chondrules, chondrule fragments, calcium–aluminum inclusions, amoeboid-olivine aggregates, dark inclusions,

Fe,Ni metal, and sulfides, all embedded in a fine-grained phyllosilicate-bearing matrix (Weisberg et al., 1993). These chondrites are made up of 48–63 vol% chondrules and chondrule fragments, 36–51 vol% matrix and dark inclusions (except Al Rais, which contains up to 70 vol%), and <1 vol% refractory inclusions (Weisberg et al., 1993). Most of the chondrules are type-I; it has been reported that type-II chondrules are <1 vol% of the chondrule population (Weisberg et al., 1993). All chondrule textural types (Gooding and Keil, 1981) are present. However, chondrules with non-porphyrritic textures comprise only a small fraction of the total chondrule population (Weisberg et al., 1993; Connolly et al., 2001). The majority of CRs have experienced aqueous alteration of varying intensity. Renazzo,

\* Corresponding author. Fax: +1 520 621 9692.

E-mail address: [schrader@lpl.arizona.edu](mailto:schrader@lpl.arizona.edu) (D.L. Schrader).

Al Rais, and GRO 95577 are the most aqueously altered (Weisberg et al., 1993; Weisberg and Prinz, 2000; Weisberg and Huber, 2007). Others such as MET 00426 and QUE 99177 are reported to have experienced only minimal aqueous alteration (Abreu and Brearley, 2005, 2006a,b).

While type-I chondrules in CR chondrites have been studied in detail, type-II chondrules have been relatively ignored (Krot et al., 2002; Connolly et al., 2003, 2007). Our initial investigations of type-II chondrules (Connolly et al., 2003, 2007; Schrader et al., 2007a) revealed the presence of ubiquitous sulfide phases within these chondrules as well as the chondrite matrix. Since metal and sulfides respond more readily to their environment than silicates, they are important to study in order to further our understanding of primary and secondary formation processes of the CR chondrites. Here we report the results of a detailed study of sulfide-bearing assemblages in type-II chondrules from the MAC 87320, EET 92011, and Renazzo CR carbonaceous chondrites.

## 2. EXPERIMENTAL PROCEDURE

Three thin sections (MAC 87320,10 and EET 92011,5, both from the Antarctic Meteorite Collection at Johnson Space Center, as well as Renazzo USNM1123-1, from the Smithsonian National Museum of Natural History) were selected for a detailed investigation (Table 1). The thin sections were surveyed using backscattered electron (BSE) imaging on a Hitachi S-4700 field emission gun scanning electron microscope (FEG-SEM) at the American Museum of Natural History (AMNH) with an accelerating voltage of 20 kV and beam current of 20 nA. The petrographic context of each opaque mineral was carefully documented within their host chondrule. Energy Dispersive X-Ray Spectroscopy (EDS) was used to provide an indication of the compositional variation among the assemblages. Modal

abundances of the sulfide, metal, and chromite in the chondrules were obtained using the IQmaterials<sup>®</sup> program, after first isolating images of the chondrules in the Adobe Photoshop<sup>®</sup> software package (Table 1).

Major and minor elemental abundances of the opaque phases were measured on the Cameca SX-50 electron microprobe (EMP) at the Lunar and Planetary Lab. We used an accelerating voltage of 15 kV and current of 20 nA. The elements analyzed were Fe, Ni, S, Ca, P, Co, Cr, Al, Na, Si, Mg, Mn, Ti, Zn, Cu, and O. The standards used for EMP calibration are iron metal for Fe, nickel metal for Ni, chalcopyrite for S, diopside for Ca, apatite for P, cobalt metal for Co, chromium metal for Cr, spinel for Al, albite-chromite for Na, diopside for Si, spinel for Mg, manganese metal for Mn, rutile for Ti, zinc metal for Zn, chalcopyrite for Cu, and gahnite for O. The opaque assemblages contain hydrated minerals as well as fine-grained mixtures of sulfide and oxide phases. Therefore, oxygen was measured quantitatively, as opposed to being determined by difference. Some troilite and pentlandite analyses yield O above the detection limit; this O value is not in the phase identified but rather a beam overlap. Detection limits for the EMP analyses are listed in Tables 2–4. The abundances of Al, Ca, Na, Mg, Mn, Ti, and Zn were below the detection limits for the listed analyses, and were included to identify any beam overlap with silicate phases.

## 3. RESULTS

Of the nine chondrules studied three are whole, two are chondrule fragments (those which still retain an arc permitting re-construction of the apparent diameter of the chondrule) and four are fragments (those that retain no arc but have textures suggestive of an igneous origin) (Table 1). The completeness of the chondrule was taken into con-

Table 1  
Statistics of type-II chondrules studied

Chondrule	Textural type	Mean Fa <sup>a,c,d</sup>	Shape <sup>c</sup>	Opaque area %	Number of assemblages analyzed	Number of EMP analyses
<i>MAC 87320,10</i>						
M-Ch1	PO	15.6	Fragt	2.2	3	11
M-Ch2	PO	25.8	Fragt	4.4	4	16
<i>EET 92011,5</i>						
E-Ch1	BO/Comp <sup>b</sup>	38.8	Ch Fragt	1.3	2	4
E-Ch2	PO	46.4	Ch	1.6	6	19
E-Ch4	PO	28.8	Fragt	5.6	2	3
<i>Renazzo USNM1123-1</i>						
R-Ch2	PO	45.2	Ch Fragt	8.7	1	3
R-Ch7	POP	51.7	Ch	4.1	2	5
R-Ch11	PO/GO	45.5	Ch	16.5	2	11
R-Ch13	PO	69.9 <sup>e</sup>	Fragt	13.7	2	4

Ch, chondrule; Ch Fragt, chondrule fragment; Fragt, fragment of an igneous object likely a chondrule.

<sup>a</sup> Core values for at least 3 olivine grains.

<sup>b</sup> This object is compound.

<sup>c</sup> From Connolly et al. (2001).

<sup>d</sup> From Connolly et al. (2007).

<sup>e</sup> Two grains only.

Table 2  
Wt% EMP data, MAC 87320,10

Assemblage # Analysis #	Interior or edge <sup>a</sup>	O	Na	Mg	Si	P	S	Ca	Cr	Mn	Fe	Co	Ni	Cu	Total
Fe,Ni metal															
<i>M-Ch1</i>															
A2.447	I	bdl	bdl	bdl	0.17	bdl	bdl	bdl	bdl	bdl	81.6	0.7	16.6	bdl	99.1
A2.448	I	bdl	0.05	bdl	0.05	bdl	bdl	bdl	bdl	bdl	84.0	0.7	14.6	bdl	99.5
A3.437	E	bdl	0.11	bdl	bdl	bdl	0.07	bdl	bdl	bdl	77.8	0.9	20.3	bdl	99.1
A3.438	E	bdl	bdl	bdl	bdl	bdl	bdl	bdl	bdl	bdl	80.9	1.0	17.7	bdl	99.5
A3.439	E	bdl	0.11	bdl	0.15	0.06	0.01	bdl	bdl	bdl	81.2	0.9	17.1	bdl	99.4
A4.444	E	bdl	bdl	bdl	0.12	bdl	bdl	bdl	bdl	bdl	58.6	0.7	40.0	bdl	99.4
A4.445	E	bdl	bdl	bdl	0.48	bdl	bdl	bdl	bdl	bdl	58.9	0.8	39.3	bdl	99.5
Average		bdl	0.03	bdl	0.12	0.01	0.01	bdl	bdl	bdl	74.7	0.8	23.7	bdl	99.4
Stdev		bdl	0.05	bdl	0.15	0.02	0.03	bdl	bdl	bdl	11.1	0.1	11.1	bdl	0.2
<i>M-Ch2</i>															
A1.472	I	bdl	0.05	bdl	0.16	0.51	0.05	bdl	bdl	bdl	74.0	0.8	21.8	bdl	97.4
A3.454	E	bdl	0.07	bdl	bdl	0.54	0.07	bdl	bdl	bdl	64.7	1.2	32.8	bdl	99.4
A3.462	E	bdl	0.08	bdl	0.08	0.54	0.06	bdl	bdl	bdl	61.8	1.2	34.9	bdl	98.8
Average		bdl	0.06	bdl	0.08	0.53	0.06	bdl	bdl	bdl	66.9	1.1	29.8	bdl	98.5
Stdev		bdl	0.02	bdl	0.08	0.02	0.01	bdl	bdl	bdl	6.4	0.3	7.1	bdl	1.1
Troilite															
<i>M-Ch1</i>															
A2.446	I	bdl	bdl	bdl	0.12	bdl	36.99	bdl	bdl	bdl	61.7	bdl	0.7	0.2	99.7
A2.450	I	bdl	bdl	bdl	bdl	bdl	36.49	bdl	bdl	0.07	61.6	bdl	0.5	bdl	98.7
A3.441	E	bdl	0.06	bdl	bdl	bdl	37.06	bdl	bdl	bdl	62.2	bdl	0.7	0.2	100.3
A4.442	E	bdl	bdl	bdl	0.04	bdl	36.92	0.03	bdl	bdl	62.0	bdl	0.6	0.1	99.8
Average		bdl	0.01	bdl	0.04	bdl	36.86	0.01	bdl	0.02	61.9	bdl	0.7	0.1	99.6
Stdev		bdl	0.03	bdl	0.06	bdl	0.26	0.02	bdl	0.03	0.3	bdl	0.1	0.1	0.6
<i>M-Ch2</i>															
A1.471	I	bdl	bdl	bdl	bdl	bdl	36.63	0.03	0.06	bdl	61.4	bdl	1.3	0.2	99.6
A1.474	I	bdl	bdl	bdl	0.04	bdl	36.57	bdl	bdl	bdl	61.0	bdl	1.8	bdl	99.3
A1.477	I	bdl	bdl	bdl	0.37	bdl	36.64	bdl	bdl	bdl	62.3	bdl	0.5	bdl	99.8
A2.469	E	bdl	bdl	bdl	0.03	bdl	36.95	bdl	0.07	bdl	62.1	bdl	0.5	bdl	99.6
A2.470	E	bdl	bdl	bdl	0.23	bdl	36.66	bdl	0.06	bdl	61.7	bdl	0.3	bdl	99.0
A3.455	E	bdl	bdl	bdl	0.04	bdl	36.73	bdl	bdl	bdl	62.0	bdl	0.6	0.2	99.5
A3.457	E	bdl	bdl	bdl	0.29	bdl	36.64	bdl	bdl	bdl	61.9	bdl	0.8	0.2	99.7
A3.459	E	bdl	0.05	bdl	bdl	bdl	36.54	bdl	bdl	bdl	62.2	bdl	0.6	bdl	99.4
A3.463	E	bdl	0.06	bdl	0.03	bdl	36.61	bdl	bdl	bdl	61.4	bdl	0.9	0.2	99.1
A4.465	E	bdl	bdl	bdl	bdl	bdl	36.34	bdl	0.32	bdl	61.5	0.1	0.4	0.2	98.8
A4.466	E	bdl	bdl	bdl	0.05	bdl	36.71	bdl	0.13	bdl	61.7	bdl	0.4	bdl	98.9
Average		bdl	0.01	bdl	0.10	bdl	36.64	0.00	0.06	bdl	61.7	0.0	0.7	0.1	99.4
Stdev		bdl	0.02	bdl	0.13	bdl	0.15	0.01	0.10	bdl	0.4	0.0	0.4	0.1	0.3
Phosphate															
<i>M-Ch2</i>															
A1.476	I	36.4	8.19	1.81	0.16	15.03	5.96	9.72	0.06	0.36	23.1	bdl	0.3	bdl	101.0
A1.479 <sup>b</sup>	I	40.4	8.71	4.76	1.78	17.35	0.11	3.62	1.31	0.33	22.3	bdl	0.1	bdl	100.8
Average		38.4	8.45	3.28	0.97	16.19	3.03	6.67	0.69	0.35	22.7	bdl	0.2	bdl	100.9
Stdev		2.9	0.37	2.09	1.14	1.64	4.14	4.31	0.89	0.02	0.6	bdl	0.1	bdl	0.1

Ch, chondrule; A, assemblage; bdl, below detection limit.

Detection limits are 0.11 wt% for Fe, 0.14 wt% for Ni, 0.04 wt% for S, 0.02 wt% for Ca, 0.06 wt% for P, 0.12 wt% for Co, 0.05 wt% for Cr, 0.03 wt% for Al, 0.04 wt% for Na, 0.02 wt% for Si, 0.03 wt% for Mg, 0.06 wt% for Mn, 0.03 wt% for Ti, 0.21 wt% for Zn, 0.14 wt% for Cu, and 0.70 wt% for O.

<sup>a</sup> This is the assumed location if the chondrule is not whole, as petrographic information is lacking.

<sup>b</sup> This phosphate is surrounding the assemblage.

sideration when determining the relationship between metal and sulfide phases and their petrographic context. The chondrules span a range of textural types; porphyritic oliv-

ine (PO), porphyritic olivine/pyroxene (POP), compound porphyritic olivine/barred olivine (PO/BO) chondrule pair, and porphyritic olivine/granular olivine (PO/GO), which

Table 3  
Wt% EMP data, EET 92011,5

Assemblage # Analysis #	Interior or Edge <sup>a</sup>	O	Na	Mg	Si	P	S	Ca	Cr	Mn	Fe	Co	Ni	Cu	Total
Fe,Ni metal															
<i>E-Ch2</i>															
A2.408	I	bdl	bdl	bdl	0.45	bdl	0.30	bdl	bdl	bdl	34.1	1.2	63.5	bdl	99.6
A3.411	I	bdl	0.09	bdl	0.12	bdl	bdl	bdl	bdl	bdl	35.0	1.4	61.1	bdl	97.7
A3.414	I	bdl	0.09	bdl	0.15	bdl	bdl	bdl	bdl	bdl	40.4	1.7	55.6	bdl	97.9
Average		bdl	0.06	bdl	0.24	bdl	0.10	bdl	bdl	bdl	36.5	1.4	60.1	bdl	98.4
Stdev		bdl	0.05	bdl	0.18	bdl	0.17	bdl	bdl	bdl	3.4	0.2	4.1	bdl	1.0
Troilite															
<i>E-Ch1</i>															
A3.388	I	0.7	bdl	bdl	0.12	bdl	35.94	0.05	bdl	bdl	60.4	0.4	1.4	0.2	99.1
A3.389	I	bdl	bdl	bdl	0.05	bdl	36.09	0.08	bdl	bdl	61.5	0.2	0.7	bdl	98.6
A5.385	E	bdl	bdl	bdl	bdl	bdl	36.54	bdl	bdl	bdl	62.1	bdl	0.3	0.2	99.1
A5.386	E	bdl	bdl	bdl	bdl	bdl	36.59	bdl	bdl	bdl	62.4	bdl	0.2	bdl	99.2
Average		0.2	bdl	bdl	0.04	bdl	36.29	0.03	bdl	bdl	61.6	0.1	0.6	0.1	99.0
Stdev		04	bdl	bdl	0.05	bdl	0.32	0.04	bdl	bdl	0.9	0.2	0.5	0.1	0.3
<i>E-Ch2</i>															
A1.415	I	bdl	0.05	bdl	0.16	bdl	36.82	0.03	bdl	bdl	61.6	bdl	0.3	0.2	99.1
A1.416	I	bdl	bdl	bdl	0.17	bdl	36.95	bdl	0.11	bdl	61.4	bdl	0.3	bdl	99.0
A2.405	I	bdl	bdl	bdl	0.07	bdl	36.89	bdl	bdl	0.07	62.2	bdl	0.6	bdl	99.9
A4.396	E	bdl	bdl	bdl	0.19	bdl	36.42	bdl	0.07	0.15	60.6	0.1	1.9	0.3	99.8
A4.398	E	bdl	bdl	bdl	bdl	bdl	36.68	bdl	0.09	bdl	60.2	0.2	2.2	bdl	99.4
A5.402	E	bdl	bdl	bdl	0.17	bdl	36.58	bdl	bdl	bdl	61.3	0.2	1.2	bdl	99.4
A5.403	E	bdl	bdl	bdl	0.15	bdl	36.57	bdl	0.10	bdl	61.0	0.2	1.4	bdl	99.5
A6.418	E	bdl	bdl	bdl	bdl	bdl	36.74	bdl	bdl	bdl	62.1	bdl	0.6	bdl	99.5
A6.419	E	bdl	0.05	bdl	0.08	bdl	36.54	bdl	bdl	bdl	61.6	bdl	0.7	bdl	98.9
Average		bdl	0.01	bdl	0.11	bdl	36.69	0.00	0.04	0.02	61.4	0.1	1.0	0.1	99.4
Stdev		bdl	0.02	bdl	0.07	bdl	0.18	0.01	0.05	0.05	0.6	0.1	0.7	0.1	0.3
<i>E-Ch4</i>															
A1.430	I	0.7	0.05	bdl	bdl	bdl	36.21	bdl	bdl	0.03	61.8	bdl	0.8	bdl	99.7
Pentlandite															
<i>E-Ch2</i>															
A2.406	I	bdl	bdl	bdl	0.11	bdl	33.68	bdl	0.09	bdl	42.7	0.7	21.5	0.2	99.0
A2.410	I	bdl	0.06	bdl	0.51	bdl	33.80	bdl	bdl	bdl	43.0	0.6	21.7	0.2	100.0
A4.395	E	bdl	bdl	bdl	0.05	bdl	33.57	bdl	bdl	bdl	38.4	0.7	26.7	bdl	99.4
A4.399	E	bdl	0.05	bdl	0.62	bdl	33.11	bdl	bdl	bdl	36.7	0.8	28.6	0.1	100.0
A6.420	E	bdl	bdl	bdl	0.20	bdl	33.18	bdl	bdl	bdl	36.1	0.8	29.0	0.2	99.5
A6.421	E	bdl	bdl	bdl	0.11	bdl	33.54	bdl	bdl	bdl	37.7	0.7	28.3	bdl	100.4

Opaque phases in type-II chondrules from CR2 chondrites

(continued on next page)

Table 3 (continued)

Assemblage # Analysis #	Interior or Edge <sup>a</sup>	O	Na	Mg	Si	P	S	Ca	Cr	Mn	Fe	Co	Ni	Cu	Total
Average		bdl	0.02	bdl	0.27	bdl	33.48	bdl	0.01	bdl	39.1	0.7	26.0	0.1	99.7
Stdev		bdl	0.03	bdl	0.24	bdl	0.28	bdl	0.04	bdl	3.0	0.1	3.5	0.1	0.5
<i>E-Ch4</i>															
A1.432	I	bdl	bdl	bdl	0.23	bdl	33.21	bdl	bdl	bdl	35.3	0.7	28.1	bdl	97.5
A2.424	E	bdl	0.09	bdl	bdl	bdl	33.21	bdl	bdl	bdl	35.4	0.6	29.0	0.2	98.5
Average		bdl	0.05	bdl	0.12	bdl	33.21	bdl	bdl	bdl	35.3	0.6	28.6	0.1	98.0
Stdev		bdl	0.07	bdl	0.16	bdl	0.00	bdl	bdl	bdl	0.1	0.1	0.7	0.1	0.7
Pentlandite + Oxide/Hydroxide															
<i>E-Ch2</i>															
A1.417	I	7.2	2.50	0.12	0.39	bdl	30.53	0.04	0.15	bdl	34.0	1.2	22.4	1.1	99.7

Ch, chondrule; A, assemblage; bdl, below detection limit.

Detection limits are 0.11 wt% for Fe, 0.14 wt% for Ni, 0.04 wt% for S, 0.02 wt% for Ca, 0.06 wt% for P, 0.12 wt% for Cr, 0.03 wt% for Co, 0.05 wt% for Mn, 0.04 wt% for Al, 0.04 wt% for Na, 0.02 wt% for Si, 0.03 wt% for Mg, 0.06 wt% for Mn, 0.03 wt% for Ti, 0.21 wt% for Zn, 0.14 wt% for Cu, and 0.70 wt% for O.

<sup>a</sup> This is the assumed location if the chondrule is not whole, as petrographic information is lacking.

display a large range of metal and sulfide abundances and textures (Table 1 and Figs. 1 and 2).

Tables 2–4 list the EMP analyses that were obtained over 24 sulfide-rich assemblages from the nine type-II chondrules with totals between 98 and 101 wt%. The term assemblage refers to an individual opaque object, which commonly consists of multiple phases. Mineral phases are identified using the cation/S ratios, total O abundance, cation/O ratios, and the O/S ratios from EMP data (Table 2–4). The minerals identified in this study are Fe,Ni metal, troilite, pentlandite, tochilinite, magnetite, and various phosphates. Plotting these data on an O–S–Cations ternary diagram (Fig. 3) reveals the compositional relationships among the different analyses. In this diagram, compositions resulting from the electron beam overlap of multiple phases plot in between the two end-member phases. Data points which overlap multiple phases are common in this study because the minerals in these assemblages are fine grained and intimately mixed with other phases on scales smaller than the interaction volume of the EMP beam. A large portion of troilite and pentlandite is intimately mixed with other minerals, likely tochilinite and magnetite. The mineral abundances and morphologies of the opaque assemblages are highly variable among the three meteorites studied. We present results from each meteorite in detail below.

### 3.1. MAC 87320,10: type-II chondrule opaques

Twenty-seven data points covering seven sulfide assemblages from two type-II chondrules (M-Ch1 and M-Ch2) of MAC 87320 were obtained (Table 2 and Figs. 1a, b and 4). The chondrules studied are both PO fragments (Table 1). The sulfide assemblages are dispersed throughout the chondrules. The majority of these assemblages are concentrated near the edge of M-Ch1 (Fig. 1a). Since M-Ch2 (Fig. 1b) is a chondrule fragment, it is difficult to discern the original spatial distribution of sulfides. The abundances of opaque assemblages are 2.2 (M-Ch1) and 4.4 (M-Ch2) area%. The assemblages greatly vary in morphology and composition from one another; appearing both rounded and irregular, with apparent diameters ranging from 1 to 200  $\mu\text{m}$ .

Overall, MAC 87320's type-II chondrules contain troilite, phosphate, and Ni-rich metal in complex assemblages (Table 2). The assemblages labeled A2, A3, and A4 from M-Ch1 contain Ni-rich metal grains that are partially surrounded by troilite. In both cases an angular mineral containing Fe, Ni, O, and minor S occurs in the center of each metal grain but low totals from the EMP analyses hamper identification of this phase (Table 2 and Fig. 4a). The metal in these assemblages contain up to 40 wt% Ni (Table 2), much higher than the 8.3 wt% Ni previously reported for the maximum Ni content in this meteorite (Weisberg et al., 1993).

The assemblages A1, A2, and A3 in M-Ch2 are morphologically complex (Table 2 and Fig. 4b). They contain numerous rounded Ni-rich metal blebs surrounded by troilite (Fig. 4b). M-Ch2-A1 and M-Ch2-A3 contain rounded and sub-rounded phosphate inclusions in the troilite, which has 0.32–1.76 wt% Ni. In addition, phosphate also forms a

Table 4  
Wt% EMP data, Renazzo USNM1123-1

Assemblage # Analysis #	Interior or edge <sup>a</sup>	O	Na	Mg	Si	P	S	Ca	Cr	Mn	Fe	Co	Ni	Cu	Total
<b>Pentlandite</b>															
<i>R-Ch7</i>															
A3.349	E	1.0	0.11	bdl	0.34	bdl	33.25	bdl	bdl	bdl	37.3	1.4	27.1	bdl	100.6
A3.352	E	0.8	0.05	bdl	0.03	bdl	33.43	bdl	bdl	bdl	37.1	1.4	28.0	bdl	100.8
Average		0.9	0.08	bdl	0.19	bdl	33.34	bdl	bdl	bdl	37.2	1.4	27.5	bdl	100.7
Stdev		0.1	0.05	bdl	0.22	bdl	0.13	bdl	bdl	bdl	0.1	0.0	0.6	bdl	0.2
<i>R-Ch11</i>															
A2.300	E	0.8	bdl	bdl	0.06	bdl	33.59	bdl	bdl	bdl	36.0	0.9	28.7	bdl	100.1
A2.313	E	0.9	0.07	bdl	0.21	bdl	33.17	bdl	bdl	bdl	35.9	0.9	28.5	bdl	99.6
A2.310	E	0.9	0.06	bdl	0.29	bdl	33.52	bdl	bdl	bdl	36.4	0.8	29.1	bdl	101.0
A2.306	E	0.9	0.05	bdl	0.17	bdl	33.68	bdl	bdl	bdl	36.2	0.9	28.6	bdl	100.6
A2.304	E	0.9	bdl	bdl	0.05	bdl	33.33	bdl	bdl	bdl	35.9	1.0	29.0	bdl	100.2
Average		0.9	0.03	bdl	0.15	bdl	33.46	bdl	bdl	bdl	36.1	0.9	28.8	bdl	100.3
Stdev		0.0	0.03	bdl	0.10	bdl	0.21	bdl	bdl	bdl	0.2	0.1	0.2	bdl	0.5
<i>R-Ch13</i>															
A1.341	E	1.0	0.10	bdl	0.63	bdl	33.36	bdl	bdl	bdl	35.9	0.9	28.9	bdl	100.7
A2.347	E	0.9	0.05	bdl	0.16	bdl	33.21	bdl	bdl	bdl	35.8	0.6	29.5	bdl	100.2
Average		0.9	0.08	bdl	0.40	bdl	33.29	bdl	bdl	bdl	35.8	0.7	29.2	bdl	100.4
Stdev		0.0	0.04	bdl	0.33	bdl	0.10	bdl	bdl	bdl	0.1	0.2	0.5	bdl	0.3
<b>Troilite + Oxide/Hydroxide</b>															
<i>R-Ch2</i>															
A3.369	E	6.7	0.09	bdl	0.15	bdl	31.61	0.04	bdl	bdl	62.1	bdl	0.7	bdl	101.4
A3.371	E	3.9	0.07	bdl	0.22	bdl	33.52	bdl	bdl	bdl	62.3	bdl	0.3	bdl	100.3
Average		5.3	0.08	bdl	0.18	bdl	32.57	0.02	bdl	bdl	62.2	bdl	0.5	bdl	100.8
Stdev		1.9	0.01	bdl	0.05	bdl	1.35	0.03	bdl	bdl	0.1	bdl	0.3	bdl	0.7
<i>R-Ch7</i>															
A3.351	E	2.0	bdl	0.06	0.32	bdl	34.44	bdl	0.06	bdl	61.5	bdl	0.4	bdl	98.8
A4.355	E	3.1	0.11	bdl	bdl	bdl	34.33	0.09	bdl	bdl	57.3	0.1	4.5	bdl	99.5
Average		2.5	0.05	0.03	0.16	bdl	34.38	0.05	0.03	bdl	59.4	0.1	2.4	bdl	99.1
Stdev		0.7	0.08	0.04	0.23	bdl	0.08	0.07	0.03	bdl	3.0	0.1	2.9	bdl	0.5

(continued on next page)

Opaque phases in type-II chondrules from CR2 chondrites

Table 4 (continued)

Assemblage # Analysis #	Interior or edge <sup>a</sup>	O	Na	Mg	Si	P	S	Ca	Cr	Mn	Fe	Co	Ni	Cu	Total
<i>R-Ch11</i>															
A2.305	E	2.4	0.06	bdl	bdl	bdl	35.33	bdl	bdl	bdl	62.9	bdl	0.6	bdl	101.2
A2.308	E	4.5	0.07	bdl	0.20	bdl	33.62	bdl	bdl	bdl	62.5	bdl	0.6	bdl	101.5
A3.318	E	5.2	bdl	bdl	0.42	bdl	32.30	0.03	bdl	bdl	62.1	bdl	0.6	bdl	100.7
Average		4.0	0.04	bdl	0.21	bdl	33.75	0.01	bdl	bdl	62.5	bdl	0.6	bdl	101.1
Stdev		1.5	0.04	bdl	0.21	bdl	1.52	0.02	bdl	bdl	0.4	bdl	0.0	bdl	0.4
Pentlandite + Oxide/Hydroxide															
<i>R-Ch13</i>															
A1.345	E	4.4	0.12	0.16	0.06	bdl	32.18	bdl	0.06	bdl	36.1	1.0	24.0	0.2	98.9
Tochilinite															
<i>R-Ch11</i>															
A3.330	E	9.6	0.09	0.13	0.45	bdl	27.97	0.04	bdl	bdl	62.4	bdl	0.6	bdl	101.2
A3.321	E	10.9	0.07	bdl	0.51	bdl	24.36	bdl	bdl	bdl	64.1	bdl	0.5	bdl	100.5
Average		10.2	0.08	0.07	0.48	bdl	26.16	0.02	bdl	bdl	63.3	bdl	0.6	bdl	100.8
Stdev		0.9	0.02	0.09	0.04	bdl	2.55	0.03	bdl	bdl	1.3	bdl	0.0	bdl	0.5
Magnetite + Minor Troilite or Pentlandite															
<i>R-Ch2</i>															
A3.370	E	19.9	0.12	bdl	0.36	bdl	11.53	0.04	bdl	bdl	66.4	bdl	0.6	bdl	99.0
<i>R-Ch7</i>															
A3.350	E	27.0	0.16	0.17	0.32	bdl	1.54	0.03	bdl	0.10	67.9	bdl	0.5	bdl	97.7
<i>R-Ch11</i>															
A3.333	E	24.9	0.09	0.03	0.56	bdl	5.91	0.03	bdl	bdl	67.3	bdl	0.5	bdl	99.3
<i>R-Ch13</i>															
A1.344	E	24.5	0.34	bdl	0.38	bdl	4.27	bdl	0.07	0.27	64.5	0.2	2.6	bdl	97.1

Ch, chondrule; A, assemblage; bdl, below detection limit.

Detection limits are 0.11 wt% for Fe, 0.14 wt% for Ni, 0.04 wt% for S, 0.02 wt% for Ca, 0.06 wt% for P, 0.12 wt% for Co, 0.05 wt% for Cr, 0.03 wt% for Al, 0.04 wt% for Na, 0.02 wt% for Si, 0.03 wt% for Mg, 0.06 wt% for Mn, 0.03 wt% for Ti, 0.21 wt% for Zn, 0.14 wt% for Cu, and 0.70 wt% for O.

<sup>a</sup> This is the assumed location if the chondrule is not whole, as petrographic information is lacking.

partial rim that surrounds the assemblages (Fig. 4b). The Ni-rich metal blebs contain 22–35 wt% Ni (Table 2).

### 3.2. EET 92011,5: type-II chondrule opaques

We obtained twenty-six analyses from ten sulfide assemblages in three type-II chondrules (E-Ch1, E-Ch2, and E-

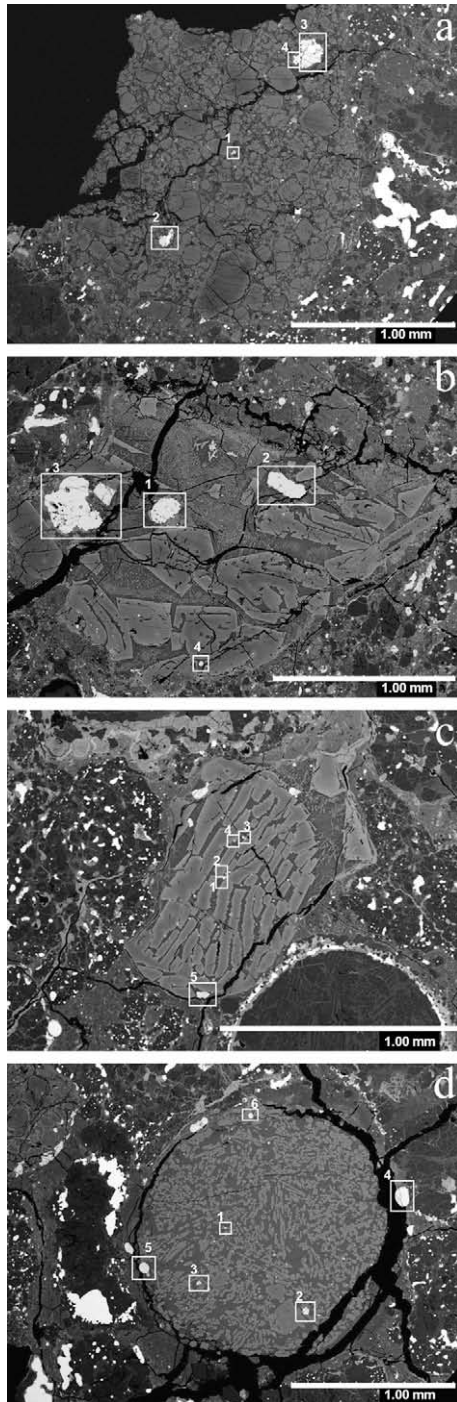


Fig. 1. BSE images of MAC 87320,10 (M) and EET 92011,5 (E) type-II chondrules, with each chondrule's sulfide-rich assemblages labeled. The boxed and numbered areas refer to the assemblage number. (a) M-Ch1: a porphyritic olivine chondrule, at the edge of the thin section. (b) M-Ch2: a porphyritic olivine chondrule. (c) E-Ch1: a barred olivine/compound chondrule. This is the only compound and the only barred olivine chondrule seen in this study. (d) E-Ch2: a porphyritic olivine chondrule. Assemblage 2 contains the most Ni-rich Fe,Ni metal observed in CR chondrites.

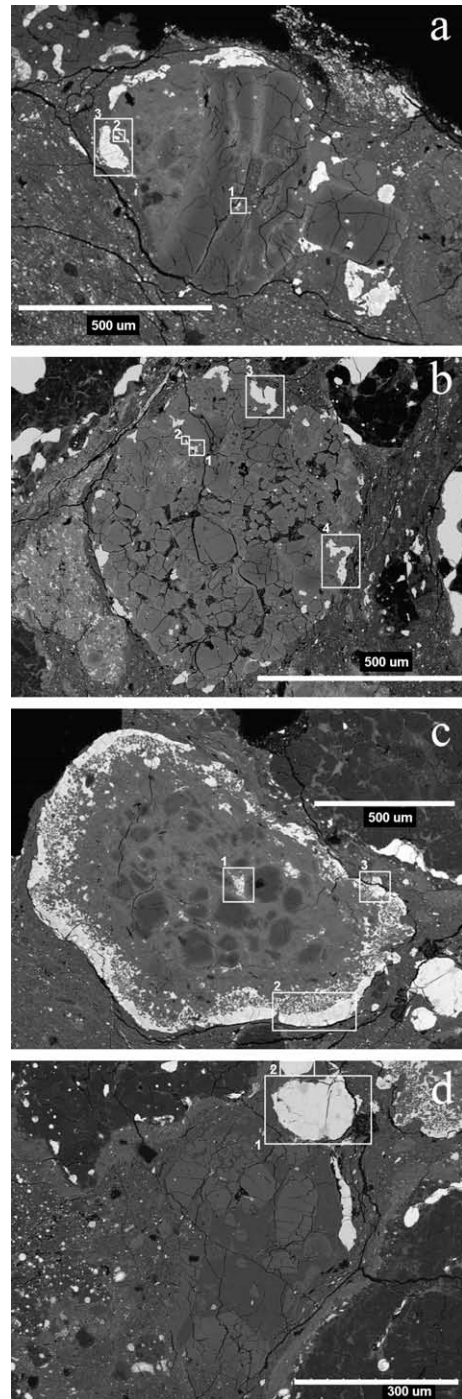


Fig. 2. Back-scattered electron (BSE) images of Renazzo USNM1123-1 (R) chondrules, with each chondrule's sulfide-rich assemblages labeled. The boxed and numbered areas refer to the assemblage number. (a) R-Ch2: a porphyritic olivine chondrule. (b) R-Ch7: a porphyritic olivine pyroxene chondrule. (c) R-Ch11: a porphyritic olivine/granular olivine chondrule. This is the most opaque-rich chondrule in this study. (d) R-Ch13: a porphyritic olivine chondrule.

Ch4) in EET 92011 (Table 3 and Figs. 1c, d and 5). We studied one BO-compound chondrule and two PO chondrules (Table 1). The opaque assemblages are present throughout the chondrules, but are concentrated near their edges. The assemblages are fine-grained mixtures of predominantly pentlandite, troilite, and Ni-rich metal (Table 3). They are either rounded or irregular and range in size from 1 to 100  $\mu\text{m}$  along their longest dimension. The modal abundances of opaque assemblages are 1.3 (E-Ch1), 1.6 (E-Ch2), and 5.6 (E-Ch4) area% (Table 1).

E-Ch1 is the only BO-compound chondrule in this study. It contains troilite-bearing assemblages (Table 3 and Figs. 1c and 5a, b). E-Ch1-A4 is completely encased in an olivine crystal (Fig. 5a). All other assemblages occur in the chondrule mesostasis (Fig. 5). The majority of the assemblages in the interior of E-Ch1 are rounded and small, while those along the chondrule edge are irregular and larger (Fig. 1c). While they contain low totals, assemblages near the edge of the chondrule are Ni-rich iron-sulfides, suggesting that intimately mixed pentlandite may be present at the edge of the chondrule.

E-Ch2 contains the most complex sulfide-rich assemblages in EET 92011 (Table 3 and Figs. 1d and 5c–f). It is a PO chondrule and contains high Ni metal, troilite, pentlandite, and O-bearing material, possibly magnetite or tochilinite. Analyses of the O-bearing material is difficult because it is fine-grained, resulting in beam overlap with nearby pentlandite. E-Ch2-A2 is rounded and contains the most Ni-rich metal yet observed in a CR chondrite with 63.5 wt% Ni. The metal is surrounded by troilite with 0.6 wt% Ni and has subhedral pentlandite along its edges (Table 3 and Fig. 5d). E-Ch2-A5 is similar to E-Ch2-A2 because it is rounded, contains troilite, and possibly pentlandite, though these analyses produced data with low totals, but it lacks metal (Fig. 5f). Ni-rich metal is only present in the assemblages in the chondrule interior (E-Ch2-A2 and E-Ch2-A3) (Table 3, Figs. 1d and 5d).

E-Ch4 contains troilite and pentlandite (Table 3). E-Ch4-A1 occurs in the interior of the chondrule fragment and is

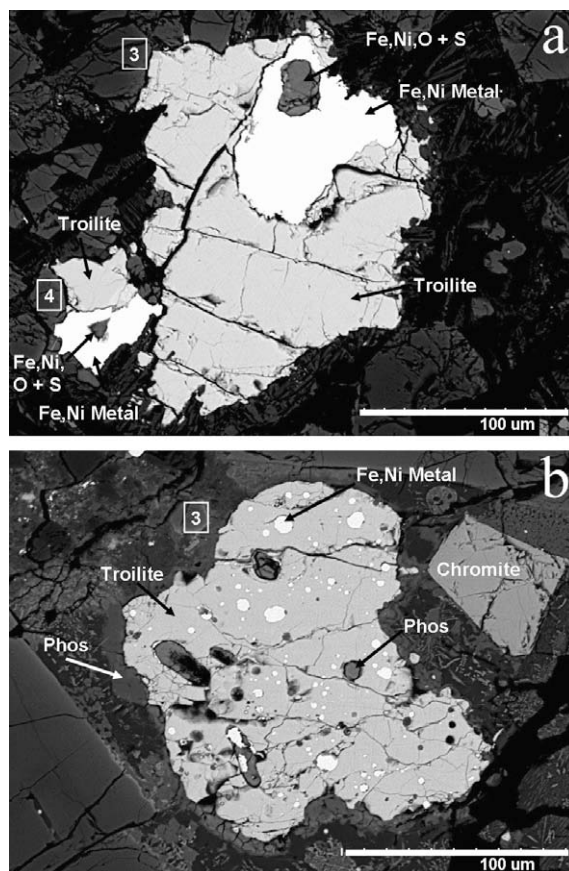


Fig. 4. BSE images of sulfide-rich assemblages in MAC 87320,10. Phos = phosphate. (a) M-Ch1 Assemblages 3 and 4: contain a Fe, Ni, O, and minor S bearing mineral, surrounded by Ni-rich metal, and partially surrounded by Ni-bearing troilite. (b) M-Ch2 Assemblage 3: contains phosphates and Ni-rich metal, both surrounded by Ni-bearing troilite. The entire assemblage is surrounded by phosphate.

composed of troilite and pentlandite. E-Ch4-A2 is along the chondrule edge, and contains pentlandite (Table 3).

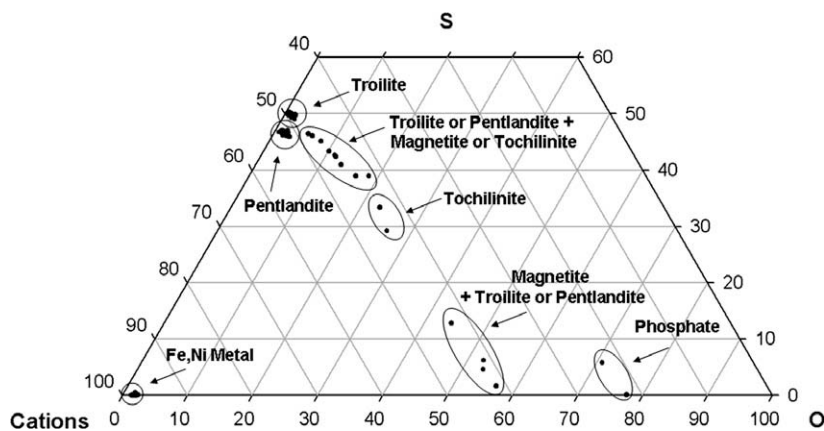


Fig. 3. Ternary diagram plotting atomic percent oxygen–sulfur–cations of all of the normalized electron microprobe analyses from MAC 87320,10, EET 92011,5, and Renazzo USNM1123-1, and labeled by mineral grouping; Cations = Fe + Ni + Co + Cu + Cr + Mn + Zn + Ca + Al + Mg. The region that plots between the end-member phases of troilite/pentlandite and magnetite, results from the electron beam overlap of those phases, and possibly tochilinite.

### 3.3. Renazzo USNM1123-1: type-II chondrule opaques

Twenty-three data points, covering seven sulfide assemblages from four type-II chondrules (R-Ch2, R-Ch7, R-Ch11, and R-Ch13), of Renazzo were obtained (Table 4 and Figs. 2 and 6). The chondrules studied include two PO, one POP, and one PO/GO (Table 1). The sulfide assemblages are dispersed throughout the chondrules with a greater concentration near the chondrule edges (Fig. 2), with chondrule R-Ch11 being an extreme example of this distribution (Fig. 2c).

The assemblages in Renazzo vary in both morphology and composition (Table 4 and Fig. 6). The assemblages are rounded or irregular in shape and range in size from 1 to 150  $\mu\text{m}$  along their longest apparent axis. Modal abundances range from 4.1 to 16.5 area% (Table 1). This concentration is the highest percentage of opaque material observed in type-II chondrules in this study.

R-Ch11-A3 contains a hydroxide mineral with a composition consistent with tochilinite. Confirmation that this hydrated sulfide mineral is tochilinite requires detailed analysis of its crystal structure, which is the subject of a

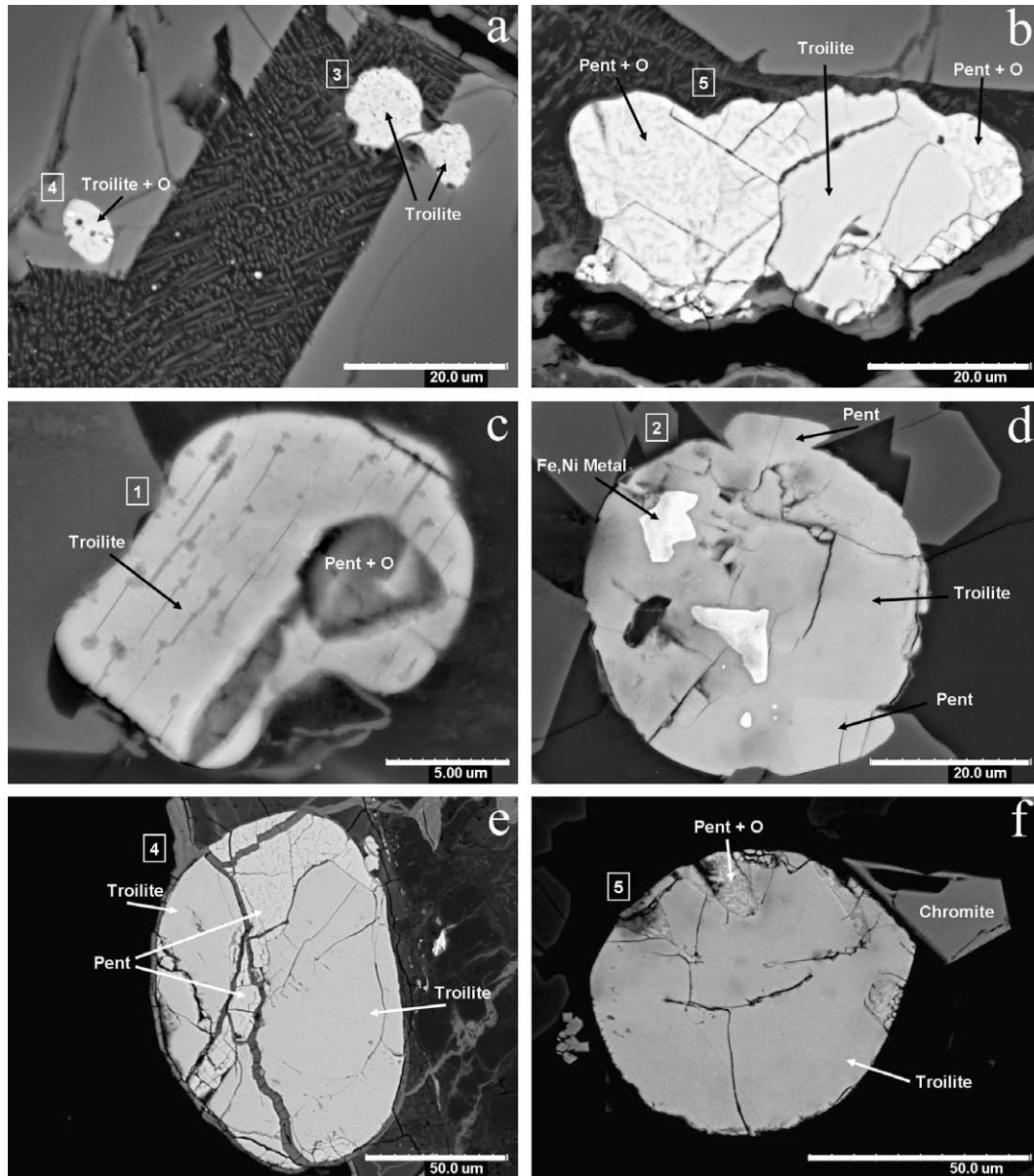


Fig. 5. BSE images of sulfide-rich assemblages in EET 92011,5. Pent = pentlandite, Pent + O = beam overlap of pentlandite and an O bearing phase. (a) E-Ch1 Assemblages 3 and 4: contain troilite and are present within olivine and the mesostasis. (b) E-Ch1 Assemblage 5: contain troilite and pentlandite + O. (c) E-Ch2 Assemblage 1: contains pentlandite + O surrounded by troilite. The dark parallel veins are most likely pentlandite. (d) E-Ch2 Assemblage 2: displays a rounded shape suggesting it was at one time molten and contains the most Ni-rich Fe,Ni metal observed in a CR. (e) E-Ch2 Assemblage 4: contains troilite and pentlandite, with pentlandite along a crack through the assemblage. (f) E-Ch2 Assemblage 5: morphologically similar to Assemblage 2, but lacks metal.

future investigation. For convenience, we will refer to this mineral as tochilinite throughout this manuscript. Tochilinite is fine grained and intimately mixed with troilite and/or magnetite (Fig. 6c), making identification of these phases difficult. In addition, R-Ch11-A3 also contains pentlandite and phosphate (Table 4 and Fig. 6c).

Chondrule R-Ch2 contains fine-grained mixtures of troilite and magnetite (Table 4 and Fig. 2a). R-Ch2-A3 is along the edge of the chondrule and is composed of troilite, and magnetite (Table 4). The magnetite is only present in an assemblage near the chondrule edge. Pentlandite may also be present, but we were unable to obtain a definitive analysis.

Chondrule R-Ch7 contains pentlandite, troilite, and magnetite (Table 4 and Figs. 2b and 6a). R-Ch7-A1-4 contains troilite, and magnetite. In R-Ch7-A3, pentlandite is present as irregular grains surrounded by troilite and magnetite (Fig. 6a).

Chondrule R-Ch11's assemblages contain tochilinite, pentlandite, magnetite, troilite, and phosphate, all of the opaque phases observed in Renazzo's type-II chondrules (Table 4 and Figs. 2c and 6b, c). The assemblages are highly concentrated near the chondrule margin, but are also present in decreasing abundance from the chondrule edge to the

interior (Figs. 2c and 6b). R-Ch11-A3 occurs along the chondrule margin and is the only assemblage observed in Renazzo to contain Ca-bearing phosphates, which are present as minor euhedral to subhedral grains enclosed within tochilinite, troilite, and magnetite (Fig. 6c). The magnetite is fine grained, mixed with troilite, and is concentrated along the chondrule edge. Large rounded pentlandite grains are concentrated along the outermost portion of the sulfides which are along the chondrule edge in R-Ch11-A2 (Fig. 6b). Irregular shaped pentlandite grains are present interior to the sulfides which are along the edge of the chondrule in R-Ch11-A2 (Fig. 6b). Analyses of the interior assemblages have low totals. The resulting analyses suggest that the electron beam overlapped troilite with magnetite or tochilinite. The resulting compositions are similar to those of assemblages occurring along the chondrule edge (Table 4).

Chondrule R-Ch13 contains pentlandite, and magnetite (Table 4 and Figs. 2c and 6d). Analyses suggest the presence of troilite, but the totals are too low for definitive identification. An EMP analysis which is the result of magnetite overlapped with troilite or pentlandite is present along the edge of R-Ch13-A1. The majority of R-Ch13-A1 and

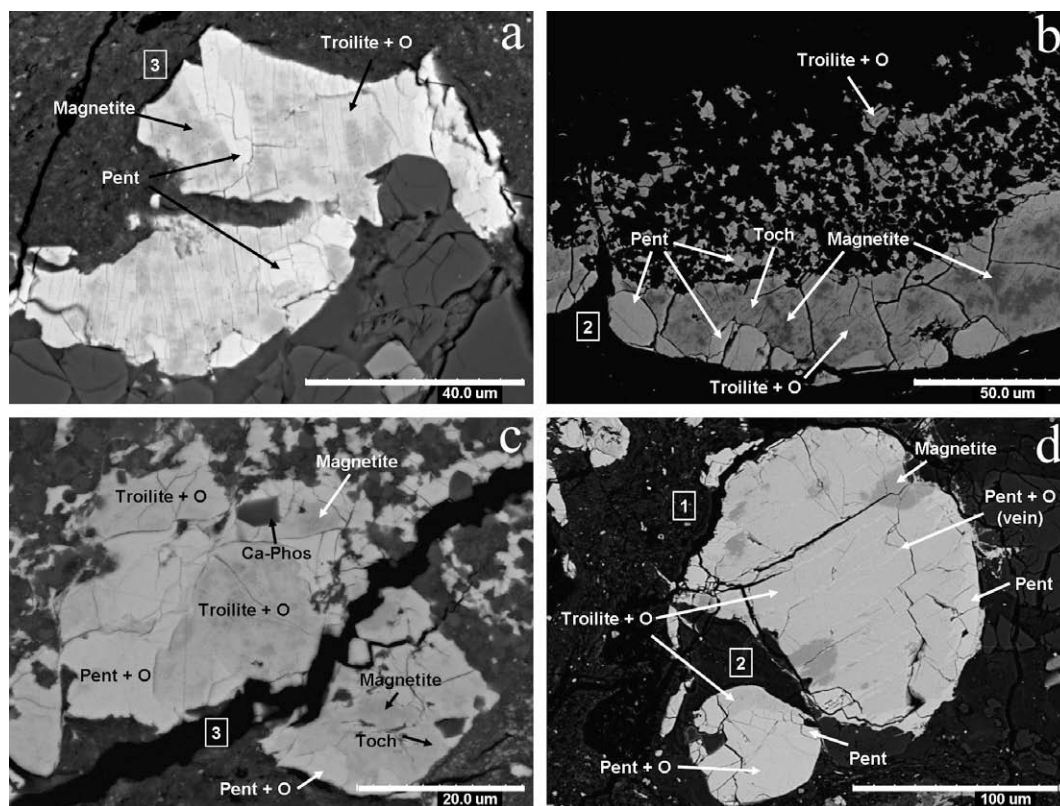


Fig. 6. BSE images of sulfide-rich assemblages in Renazzo USNM1123-1. Toch = tochilinite, Pent = pentlandite, Pent or Troilite + O = beam overlap of pentlandite or troilite and an O bearing phase, and Ca-Phos = Ca-phosphate. (a) R-Ch7 Assemblage 3: pentlandite is present as grains surrounded by magnetite and troilite + O. (b) R-Ch11 Assemblage 2: a section of an opaque which runs along the entire edge of the chondrule, with pentlandite surrounded by magnetite, tochilinite, and troilite + O. The dark area surrounding the opaque is silicate. (c) R-Ch11 Assemblage 3: occurs along the chondrule edge. Compositionally, it contains the closest match to tochilinite. It also contains pentlandite + O, troilite + O, magnetite and euhedral Ca-phosphates. (d) R-Ch13 Assemblages 1 and 2: pentlandite occurs along the edge of each assemblage, dark patches are magnetite, and the majority of the sample is troilite + O. The bright veins that are parallel along Assemblage 1 are pentlandite + O.

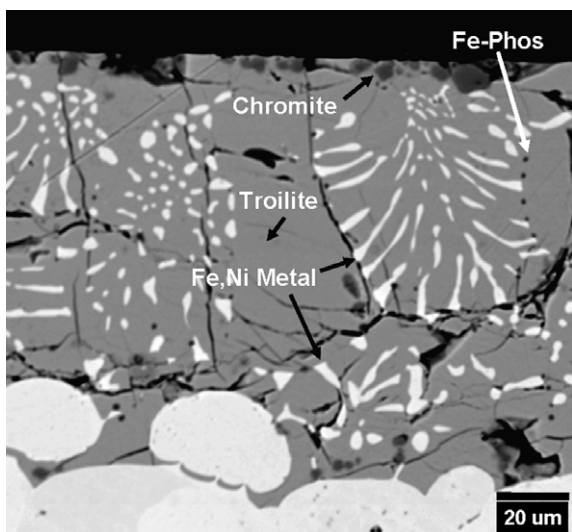


Fig. 7. BSE partial cross-sectional image of experimental product AC12-20 from Schrader et al. (2006), formed by oxidation-sulfidation of an Fe–Ni–Cr–Co–P alloy in an  $H_2$ – $H_2S$ – $CO_2$  gas mixture at 1000 °C. Fe-Phos = Fe-phosphate. The metal at the base of the figure is the remaining, unreacted Fe-alloy foil. Elongated Ni-rich metal blebs are the most Ni-rich, and rounded Fe-phosphates form near their tips.

R-Ch13-A2 appear to be troilite and pentlandite, with minor amounts of magnetite and/or tochilinite. Pentlandite is present along portions of the outer edge of R-Ch13-A1 and R-Ch13-A2 and the parallel veins in R-Ch13-A1 are pentlandite (Fig. 6d).

#### 4. DISCUSSION

Type-II chondrules from CR chondrites contain complex sulfide-rich assemblages. The morphology and composition of these assemblages suggests that they experienced varying degrees of alteration within distinctly different environments. Minerals reflective of high-temperature nebular corrosion such as troilite, phosphate and Fe,Ni metal are present in MAC 87320 and EET 92011. Minerals resulting from aqueous alteration (pentlandite, magnetite, and tochilinite) are absent in MAC 87230. These phases occur in EET 92011 and Renazzo to varying degrees. Pentlandite is present in both EET 92011 and Renazzo. Tochilinite is present in Renazzo. This phase may be present in EET 92011, as suggested by analyses of fine-grained material, which reveal significant O concentration, but definitive identification is lacking. Magnetite is only observed in Renazzo.

We interpret these results to suggest that the degree of aqueous alteration of opaque assemblages ranges from minimal alteration of MAC 87320 to extensive alteration of Renazzo. This variation in opaque mineralogy is consistent with the abundance of phyllosilicates in these meteorites (Weisberg et al., 1993). The opaque assemblages across these meteorites can thus provide insight into both the high-temperature processes associated with chondrule formation and the low-temperature processes that occurred

during aqueous alteration of the CR-chondrite parent asteroid.

#### 4.1 Gas–solid reactions during chondrule formation

The troilite in CR type-II chondrules contains up to 2.2 wt% Ni, and metal grains within these assemblages have Ni contents up to 63.5 wt%. Experimental studies of gas–solid reactions above the Fe–FeS eutectic (988 °C) have produced metal–sulfide assemblages that are compositionally and morphologically analogous to those observed in MAC 87320 and EET 92011 (Lauretta, 2005; Schrader et al., 2006). Compositionally, the Ni content in the troilite and the Ni-rich metal is similar between experimental products and the sulfide assemblages of this study. Morphologically, M-Ch2-A3 (Fig. 4b) is the most reminiscent of those assemblages presented in Schrader et al. (2006), although others are also analogous (Schrader et al., 2007b). M-Ch2-A3 contains rounded and elongated Ni-rich metal (avg = 33.9 wt% Ni), rounded phosphates and phosphate surrounding the assemblage, and Ni-bearing troilite (avg = 0.7 wt% Ni) (Table 2 and Fig. 4b). Similarly, the experimental products (Schrader et al., 2006, 2007b) contain rounded and elongated Ni-rich metal (31.4–49.6 wt% Ni), small rounded Fe-phosphates (Ca, Na, and other cations in the natural phosphates were not included in the experiments), and Ni-bearing troilite (0.9–1.8 wt% Ni). For comparison, a cross-section of one of the experimental products is shown in Fig. 7.

The presence of Ni-rich metal associated with Ni-bearing troilite in MAC 87320 and EET 92011 suggests high temperature corrosion during or after chondrule formation (Table 2 and 3). Thus, the sulfide assemblages in these type-II chondrules likely formed from Fe,Ni metal that underwent gas–solid sulfidation in the nebula above the Fe–FeS eutectic in regions of enhanced  $fO_2$  and  $fS_2$ , compared to canonic values (Ebel and Grossman, 2000).

Yu et al. (1994) and Lauretta et al. (2001) suggested some chondritic troilite may be the result of rapid flash heating and rapid cooling, in a region of S-rich gas in contact with chondrule metal, perhaps during chondrule formation. This idea is consistent with our observations in this study. Utilizing linear rate constants of the amount of sulfur adsorbed (grams/area/second) calculated by Schrader et al. (2006), formation times of these assemblages is estimated. Under similar conditions as the experiments (1 bar, enhanced  $fS_2$ ,  $fO_2$ , and at 1000 °C) M-Ch2-A3 (Fig. 4b) would have formed in under one second.

#### 4.2. Aqueous alteration on the CR chondrite parent body

The presence of pentlandite and its morphological setting suggests that the Ni-rich metal in the sulfide assemblages of type-II chondrules underwent aqueous alteration under oxidizing conditions. Pentlandite is present in EET 92011 and Renazzo, but is not present in MAC 87320. In each case pentlandite occurs along the edge of the sulfide assemblages, sometimes crosscutting the assemblage (i.e., Fig. 5e), and more often than not only near the edge of the chondrule.

Numerous theoretical studies have attributed the formation of pentlandite to aqueous alteration. Taylor et al. (1981) attributed the formation of pentlandite to oxidation of kamacite by aqueous alteration. They suggest that kamacite reacted with water, which liberated Ni. The Ni then reacted with troilite to produce pentlandite. Hutchison et al. (1987) attributed taenite and pentlandite observed in Semarkona's matrix to oxidation of kamacite by low-temperature aqueous alteration. Zanda et al. (1995) attributed pentlandite formation in primitive chondrites (Renazzo, Semarkona, and Allende) to recondensation from evaporation.

However, Lauretta et al. (1997, 1998) formed pentlandite experimentally by sulfidation of kamacite with  $H_2$ – $H_2S$  gas at 285–643 °C. Pentlandite that formed by aqueous alteration is indicated by it being present on the edges of the sulfides and along cracks, whereas pentlandite that formed in the nebula would be present within the sulfide assemblages (Lauretta et al., 1997). As pentlandite is not present in the least aqueously altered CR2 of this study, MAC 87320, and it is almost always present at the edge of sulfide assemblages in EET 92011 and Renazzo, we argue that it is most likely the result of aqueous alteration of Fe,Ni metal in these samples.

Fine-grained tochilinite is intimately mixed with troilite, pentlandite, and/or magnetite in Renazzo. Fe,Ni metal is absent in all of the tochilinite-bearing assemblages. The presence of tochilinite in Renazzo constrains the temperature of aqueous alteration, and its morphological setting hints at its formation process within CR chondrites. In CM chondrites, tochilinite is hypothesized to form from aqueous alteration of Fe,Ni metal by a sulfur-rich fluid (Tomeoka and Buseck, 1985; Tomeoka et al. 1989; Lauretta et al., 2000) under very reducing conditions (Browning and Bourcier, 1996). Due to the presence of serpentine and tochilinite, CM2 chondrite alteration temperatures have been estimated at below 50 °C (with low  $fO_2$  and low water/rock ratios) (Zolensky et al., 1993). Brearley (2006) noted that the upper thermal stability limit of tochilinite is around 120 °C. Yet, Kakos et al. (1994) and Kozerenko et al. (1996) experimentally formed tochilinite at temperatures up to 200 °C. Peng et al. (2007) experimentally formed Fe–Mg–Al-bearing tochilinite by hydrothermal alteration of an Fe, Mg, and Al powder with S-enriched water under reducing and basic conditions at temperatures below 200 °C, but state that tochilinite in CMs likely formed between 50 and 100 °C. Their experiments at around 200 °C formed little tochilinite, whereas experiments between 90 and 105 °C formed the most abundant tochilinite of the temperature range investigated (Peng et al., 2007). Therefore, depending on the conditions (pressure, pH,  $fO_2$ ,  $fH_2$ ,  $P_T$ , etc.) of the reaction mechanism taking place, the presence of tochilinite at the very least suggests alteration temperatures approximately between 50 and 200 °C; although a thorough study of tochilinite phase stability is needed to better constrain these conditions.

On the basis of comparison between Murchison (CM2) and Orgueil (CII), Weisberg et al. (1993) suggested an alteration temperature for the CR2 chondrites between 0 and 150 °C. Clayton and Mayeda (1977) estimated alteration

temperatures around 300 °C, based on the equilibration temperature corresponding to the oxygen isotopic fractionation between the hydrous silicate matrix and magnetite in Renazzo. This wider range of alteration temperatures for CR2s is further evidence of their complex alteration history.

The fact that tochilinite and metal are not observed to occur in the same assemblage suggests that, once started, the formation of tochilinite in CR2 chondrites went to completion. This observation suggests several possibilities: (1) the formation reaction is rapid; (2) the duration of aqueous alteration was extensive; and/or (3) the aqueously altered CR chondrites had a high water to rock ratio. Therefore, it is likely that the tochilinite in CR2s formed by sulfur-rich aqueous alteration of Fe,Ni metal at around 50–200 °C (Zolensky et al., 1993; Kakos et al., 1994; Kozerenko et al., 1996; Brearley, 2006; Peng et al., 2007).

Magnetite is only present in Renazzo and occurs in the sulfide assemblages near the edges of type-II chondrules (Table 4 and Fig. 6). The magnetite in this study is fine grained and intimately mixed with troilite or pentlandite. As Renazzo is the most heavily altered of the CR chondrites analyzed in this study, this observation suggests that magnetite is the result of a higher degree of aqueous alteration, different alteration temperature,  $fO_2$ , and/or time scale than EET 92011 or MAC 87320. The magnetite association with tochilinite in Renazzo suggests it is the product of intense aqueous alteration of Fe,Ni metal, and it may be oxidized tochilinite.

#### 4.3. Type-II vs. type-I chondrules in CR2 chondrites

A high percentage of type-II chondrules are fragments (Table 1), whereas the majority of type-I chondrules in CR2s are whole, further suggesting a different formational and/or post-formation history. This observation suggests that the region where type-II chondrules formed was either dynamically active or denser than the type-Is, a shock event occurred in the type-II region that did not affect the type-Is, or type-IIs are more brittle and/or porous than type-Is; all of which resulted in more broken chondrules.

The high percentage of broken type-II chondrules leads to the supposition that the inevitable small chondrule fragments are likely included in the matrix of CR chondrites. While type-II chondrules were likely never as abundant as type-Is prior to accretion of the CR chondrite parent body, it is possible that there were more type-IIs than are observed now. Therefore, broken up type-II chondrules could account for some of the sulfides observed in the matrix of CR chondrites, as well as the matrix itself.

CR2 type-II chondrules contain abundant sulfide phases, whereas opaque assemblages in type-I chondrules are dominated by metal (Connolly et al., 2001). This dichotomy suggests that type-II chondrules in CR chondrites either had considerably different precursors, experienced different formation environments (e.g.,  $fO_2$ ,  $fS_2$ , thermal history,  $P_T$ ), and/or experienced different post-formation and pre-accretion histories than type-Is.

Connolly et al. (2008) suggested that the precursors of type-II chondrules were in part type-I chondrules. This idea is consistent with the observations of this study. It is likely

that a small population of type-I chondrules were recycled and formed the precursors to the type-II chondrules. The type-II chondrules melted in an environment with enhanced ambient  $fO_2$  and  $fS_2$ , relative to that of type-I chondrule formation.

Another potential formation scenario is that fragmented type-I chondrules, with or without Fe,Ni metal, were mixed with a more oxidized composition similar to solar then melted (Connolly et al., 2001, 2008). These chondrules then experienced gas–solid reaction, producing the observed sulfides. In either model, the key component is type-I chondrules and the key process is a reaction between gas and solid to produce the opaque assemblages.

#### 4.4. Formation and alteration of the CR parent body

The CR chondrite parent body formed in a complex stage of heating and cooling, experienced a wide range in  $fO_2$  and  $fS_2$ , and underwent a wide range of aqueous alteration after formation. The data from this study, as well as that of previous studies (Weisberg et al., 1993; Kong and Palme, 1999; Weisberg and Prinz, 2000; Connolly et al., 2001, 2007, 2008; Abreu and Brearley, 2005, 2006a,b; Schrader et al. 2006, 2007a,b; Weisberg and Huber, 2007) has led us to propose the following model of the formation of the CR parent body (Fig. 8).

The CR parent body began as condensing dust and gas in the solar nebula (Fig. 8a). The majority of the condensing material was likely a homogeneous mixture of silicates and metals, yet it is possible that condensates primarily of metal and primarily of silicate existed. These condensates, mixed with a low  $fO_2$  and low  $fS_2$  gas, were then heated.

Type-I chondrules and their opaques formed by heating gas and dust in a reducing and non-sulfidizing (low  $fO_2$  and  $fS_2$ ) region (Fig. 8b). This environment resulted in the formation of FeO-poor silicates ( $Fa_{0.5-10.0}$  (Weisberg et al., 1993)) and Fe,Ni metal within the chondrules; very few to no sulfides formed. The majority of the metal in type-I chondrules likely formed by metal silicate fractionation by reduction of FeO in the chondrule and condensation of evaporated vapors from the chondrule during chondrule formation (Connolly et al., 2001). Some metal may have also formed by recondensation after chondrule formation. Maximum temperatures experienced by type-I chondrules were not high enough to produce many non-porphyrific chondrules; porphyritic types are dominant (Hewins and Radomsky, 1990; Weisberg et al., 1993). The opaque phase formed under these reducing conditions is Fe,Ni metal, with Ni contents ranging from 3.8 to 14.3 wt% (Weisberg et al., 1993).

Some type-I chondrules were recycled and became part of the precursors to type-II chondrules and their opaque assemblages (Connolly et al., 2008). This idea is supported by the fact that relict grains within type-II chondrules have both Fa values and O-isotope ratios that are similar to those of type-I chondrules (Connolly et al., 2008). These second-generation chondrules were melted by flash heating in an oxidizing and sulfidizing environment (enhanced  $fO_2$  and  $fS_2$  compared to canonical (Ebel and Grossman, 2000)) (Fig. 8c). Peak chondrule-forming temperatures

would have completely volatilized S. The opaque assemblages formed by corrosion of pre-existing metal above the Fe–FeS eutectic under oxidizing and sulfidizing conditions (Schrader et al., 2007a,b). This process resulted in type-II chondrules being composed of FeO-rich silicates ( $Fa_{9.75-69.9}$  (Connolly et al., 2007)), troilite, Ni-rich metal, phosphates, and chromites. The initial sulfide-rich assemblages were anhydrous.

A dynamically violent phase took place following type-II chondrule formation. This dynamical event fragmented the majority of the type-II chondrules, which resulted in rare compound chondrule associations and produced abundant chondrule fragments and small remnants of type-II chondrules (Fig. 8d). The accretion of the CR parent body may have caused the fragmentation.

The resulting chondrules and fragments, as well as a minor amount of Al-rich chondrules and refractory inclusions, accreted with the volatile rich matrix and ice grains. The chondrules and matrix of CR chondrites may have formed in the same region of the nebula (Kong and Palme 1999). As the result of accretion (Fig. 8f) and decay of radiogenic isotopes, the CR parent body experienced heating. Heating melted the water ice trapped within the parent body, which resulted in aqueous alteration. The extent of aqueous alteration is dependent on the maximum temperature reached, the duration of heating (both functions of depth within the parent body), and amount of water ice mixed in with the CR material. The resulting mineralogy is a function of the precursor compositions as well as fluid pH, oxidation state, composition, and pressure. As all CR2s are breccias (Weisberg et al., 1993), some local heating and associated aqueous alteration could also have been induced by impacts. Varying degrees of aqueous alteration occur resulting in different petrologic types (1, 2, and 3) of CR chondrites (Weisberg and Prinz, 2000; Sipiera and Cole, 2004; Smith et al., 2004; Abreu and Brearley, 2005, 2006a,b; Weisberg and Huber, 2007).

## 5. CONCLUSIONS

Type-II chondrules from CR chondrites contain complex sulfide-rich assemblages. The composition and mineral abundance of the sulfide-rich assemblages display a relationship between each of the CR chondrites. The differences in the sulfides in MAC 87320, EET 92011, and Renazzo appear to be from increasing aqueous alteration and not initial differences in the sulfides among the meteorites. The amount of tochilinite, magnetite, and pentlandite compared to the amount of Fe,Ni metal and troilite present in type-II chondrules correlates with the degree of hydration of each meteorite, which decreases from Renazzo to EET 92011 to MAC 87320.

It is likely that type-II chondrules formed from remelted type-I chondrules that experienced gas–solid reactions, where solar composition metal within the chondrules underwent oxidation or oxidation/sulfidation at temperatures above 988 °C, which formed troilite and Ni-rich metal. These assemblages then underwent aqueous alteration within the parent body to various degrees and conditions

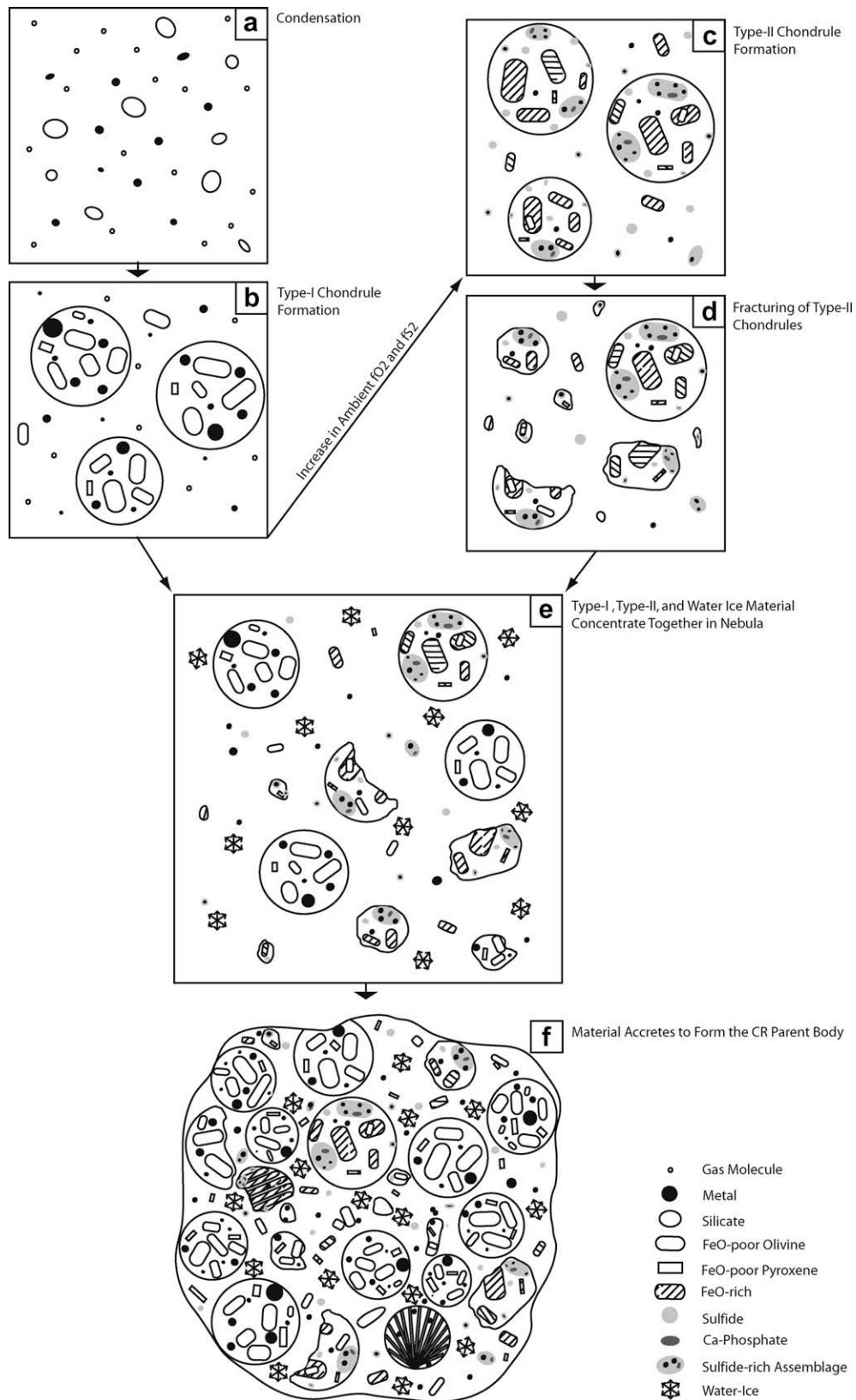


Fig. 8. CR parent body formation model. (a) CR parent body precursor material in the nebula. (b) Type-I chondrule formation. (c) Type-II chondrule formation from re-melted type-I chondrules and an increase in the ambient  $fO_2$  and  $fS_2$ . (d) Chondrule fragmentation. (e) Accumulation of type-I, type-II, and water ice material in the nebula. (f) Accretion of the CR parent body. Note: the type-I vs. type-II chondrule population shown is not representative of that in CRs, instead it was chosen to easily represent each chondrule type's history.

at temperatures ranging from around 50 to 200 °C; which produced pentlandite, tochilinite, and magnetite.

#### ACKNOWLEDGMENTS

The authors thank K. Domanik for assistance with the EMP, and J. Mey for assistance with the FEG-SEM. M.K. Weisberg and D.S. Ebel are thanked for their helpful discussions. We also thank the MWG and NMNH for the samples used in this study, as well as Sara Russell, Brigitte Zanda, and others for helpful reviews. This research was funded in part by the Carson Fellowship, NASA Grant NNG05GF39G (HCCJr, PI), NNX07AF96G (DSL, PI), and NSF-REU # AST-055258, CUNY and AMNH.

#### REFERENCES

- Abreu N. M. and Brearley A. J. (2005) Mineralogical characterization of the matrices of the primitive CR chondrites MET 00426 and EET 99177. *Meteorit. Planet. Sci.* **40**(Suppl.), 5332 (abstr.).
- Abreu N. M. and Brearley A. J. (2006a) Early solar system processes recorded in the matrices of CR2 chondrites MET 00426 and QUE 99177. *Lunar and Planet. Sci. XXXVII*. Lunar Planet. Inst., #2395 (abstr.).
- Abreu N. M. and Brearley A. J. (2006b) Onset of aqueous alteration in primitive CR chondrites. *Meteorit. Planet. Sci.* **41**(Suppl.), 5372 (abstr.).
- Brearley A. J. (2006) The action of water. In *Meteorites and the Early Solar System II* (eds. D. S. Lauretta and H. Y. McSween). University of Arizona Press, Tucson, Arizona, pp. 584–624.
- Browning L. B. and Bourcier W. L. (1996) Tochilinite: a sensitive indicator of alteration conditions on the CM asteroidal parent body. *Lunar Planet. Sci. XXVII*. Lunar Planet. Inst., 171–172 (abstr.).
- Connolly, Jr., H. C., Huss G. R. and Wassenburg G. J. (2001) On the formation of Fe–Ni metal in Renazzo-like carbonaceous chondrites. *Geochim. Cosmochim. Acta* **65**, 4567–4588.
- Connolly H. C. Jr., Weisberg M. K. and Huss G. R. (2003) On the nature and origins of FeO-rich chondrules in CR2 chondrites: a preliminary report. *Lunar Planet. Sci. XXXIV*. Lunar Planet. Inst., #1770 (abstr.).
- Connolly H. C. Jr., Weisberg M. K., Huss G. R., Nagashima K., Ebel D. S., Schrader D. L. and Lauretta D. S. (2007) On the nature of origins of type II chondrules from CR2 chondrites. *Lunar Planet. Sci. XXXVIII*. Lunar Planet. Inst., #1571 (abstr.).
- Connolly H. C. Jr., Huss G. R., Nagashima K., Weisberg M. K., Ash R. D., Ebel D. S., Schrader D. L. and Lauretta D. S. (2008) Oxygen isotopes and the nature and origins of type-II chondrules in CR2 chondrites. *Lunar Planet. Sci. XXXIX*. Lunar Planet. Inst., #1675 (abstr.).
- Clayton R. N. and Mayeda T. K. (1977) Oxygen isotopic compositions of separated fractions of the Leoville and Renazzo carbonaceous chondrites. *Meteoritics* **12**, 199.
- Ebel D. S. and Grossman L. (2000) Condensation in dust-enriched systems. *Geochim. Cosmochim. Acta* **64**, 339–366.
- Gooding J. L. and Keil K. (1981) Relative abundances of chondrule primary textural types in ordinary chondrites and their bearing on conditions of chondrule formation. *Meteoritics* **16**, 17–43.
- Hewins R. H. and Radomsky P. M. (1990) Temperature conditions for chondrule formation. *Meteoritics* **25**, 309–318.
- Hutchison R., Alexander C. M. O'D. and Barber D. J. (1987) The Semarkona meteorite: first recorded occurrence of smectite in an ordinary chondrite, and its implications. *Geochim. Cosmochim. Acta* **51**, 1875–1882.
- Kakos G. A., Turney T. W. and Williams T. B. (1994) Synthesis and structure of tochilinite: a layered metal hydroxide/sulfide composite. *J. Solid State Chem.* **108**, 102–111.
- Kong P. and Palme H. (1999) Compositional and genetic relationship between chondrules, chondrule rims, metal, and matrix in the Renazzo chondrites. *Geochim. Cosmochim. Acta* **63**, 3673–3682.
- Kozerenko S. V., Organova N. J., Fadeev V. V., Magazina L. O., Kolpakova N. N. and Kopneva L. A. (1996) *Lunar Planet. Sci. XXVII*. Lunar Planet. Inst., 695–696 (abstr.).
- Krot A. N., Anders M., Weisberg M. K. and Keil K. (2002) The CR chondrite clan: implications for early solar system processes. *Meteorit. Planet. Sci.* **37**, 1451–1490.
- Lauretta D. S., Lodders K. and Fegley, Jr., B. (1997) Experimental simulations of sulfide formation in the solar nebula. *Science* **277**, 358–360.
- Lauretta D. S., Lodders K. and Fegley, Jr., B. (1998) Kamacite sulfuration in the solar nebula. *Meteorit. Planet. Sci.* **33**, 821–833.
- Lauretta D. S., Hua X. and Buseck P. R. (2000) Mineralogy of fine-grained rims in the ALH 81002 CM chondrite. *Geochim. Cosmochim. Acta* **64**, 3263–3273.
- Lauretta D. S., Buseck P. R. and Zega T. J. (2001) Opaque minerals in the matrix of the Bishunpur (LL3.1) chondrite: constraints on the chondrule formation environment. *Geochim. Cosmochim. Acta* **65**, 1337–1353.
- Lauretta D. S. (2005) Sulfidation of an iron–nickel–chromium–cobalt–phosphorus alloy in 1% H<sub>2</sub>S–H<sub>2</sub> gas mixtures at 400–1000 °C. *Oxid. Met.* **64**, 1–22.
- McSween H. Y. (1979) Are carbonaceous chondrites primitive or processed? *Rev. Geophys. Space Phys.* **17**, 1059–1078.
- Nelen J., Kurat G. and Fredriksson K. (1975) The Renazzo chondrite—a reevaluation. *Meteoritics* **10**, 464–465.
- Peng Y., Xu L., Xi G., Zhong C., Lu J., Meng Z., Li G., Zhang S., Zhang G. and Qian Y. (2007) An experimental study on the hydrothermal preparation of tochilinite nanotubes and tochilinite-serpentine-intergrowth nanotubes from metal particles. *Geochim. Cosmochim. Acta* **71**, 2858–2875.
- Schrader D. L., Schmidt B. E. and Lauretta D. S. (2006) Oxidation and sulfidation–oxidation of Fe-based Alloys in H<sub>2</sub>–H<sub>2</sub>S–CO<sub>2</sub> gas mixtures. *Lunar Planet. Sci. XXXVII*. Lunar Planet. Inst., #2256 (abstr.).
- Schrader D. L., Connolly H. C. Jr., Lauretta D. S., Weisberg M. K. and Ebel D. S. (2007a) Characterization of opaque phases in type-II chondrules from CR2 chondrites. *Lunar Planet. Sci. XXXVIII*. Lunar Planet. Inst., #1368 (abstr.).
- Schrader D. L., Lauretta D. S. and Connolly, Jr., H. C. (2007b) Sulfide-rich assemblages in CR type-II chondrules formed by high-temperature gas–solid reaction. *Meteorit. Planet. Sci.* **42**(Suppl.), 5244 (abstr.).
- Sipiera P. P. and Cole K. J. (2004) A first look at Acfer 324: evidence for another CR 3 chondrite? *Lunar Planet. Sci. XXXV*. Lunar Planet. Inst., #1063 (abstr.).
- Smith C. L., Russell S. S., Gounelle M., Greenwood R. C. and Franchi I. A. (2004) NWA 1152 and Sahara 00182: new primitive carbonaceous chondrites with affinities to the CR and CV groups. *Meteorit. Planet. Sci.* **39**, 2009–2032.
- Taylor G. J., Okada A., Scott E. R. D., Rubin A. E., Huss G. R. and Keil K. (1981) The occurrence and implications of carbide–magnetite assemblages in unequilibrated ordinary chondrites. *Lunar Planet. Sci. XII*. Lunar Planet. Inst., 1076–1078 (abstr.).
- Tomeoka K. and Buseck P. R. (1985) Indicators of aqueous alteration in CM carbonaceous chondrites: microtextures of a layered mineral containing Fe, S, O and Ni. *Geochim. Cosmochim. Acta* **49**, 2149–2163.

- Tomeoka K., McSween H. Y. and Buseck P. R. (1989) Mineralogical alteration of CM chondrites: a review. *Proc. NIPR Symp. Antarct. Meteorites* **2**, 221–234.
- Weisberg M. K., Prinz M., Clayton R. N. and Mayeda T. K. (1993) The CR (Renazzo-like) carbonaceous chondrite group and its implications. *Geochim. Cosmochim. Acta* **57**, 1567–1586.
- Weisberg M. K. and Prinz M. (2000) The Grosvenor Mountains 95577 CR1 chondrite and hydration of the CR chondrites. *Meteorit. Planet. Sci.* **35**(Suppl.), A168 (abstr.).
- Weisberg M. K. and Huber H. (2007) The GRO 95577 CR1 chondrite and hydration of the CR parent body. *Meteorit. Planet. Sci.* **42**, 1495–1503.
- Yu Y., Hewins R. H., Zanda B. and Connolly H. C. (1994) Can sulfide minerals survive the chondrule-forming transient heating event? *Lunar Planet. Sci. XXV*. Lunar Planet. Inst., 1537–1538 (abstr.).
- Zanda B., Bourot-Denise M. and Hewins R. H. (1995) Condensate sulfide and its metamorphic transformations in primitive chondrites. *Meteoritics* **30**, 605 (abstr.).
- Zolensky M., Barrett R. and Browning L. (1993) Mineralogy and composition of matrix and chondrule rims in carbonaceous chondrites. *Geochim. Cosmochim. Acta* **57**, 3123–3148.

*Associate editor:* Sara S. Russell